MIT Open Access Articles

Controllable Perovskite Crystallization via Antisolvent Technique Using Chloride Additives for Highly Efficient Planar Perovskite Solar Cells

Controllable Perovskite Crystallization via Anti-Solvent Technique Using Chloride Additives for Highly Efficient Planar Perovskite Solar Cells

Mohammad Mahdi Tavakoli[1]*, Pankaj Yadav[2], Daniel Prochowicz[3], Melany Sponseller[1], Anna Osherov[1], Vladimir Bulović[1], Jing Kong[1]*

[1]Department of Electrical Engineering and Computer Science, Massachusetts Institute of Technology, Cambridge, MA, USA

[2]Department of Solar Energy, School of Technology, Pandit Deendayal Petroleum University, Gandhinagar-382 007, Gujarat, India

[3]Institute of Physical Chemistry, Polish Academy of Sciences, Kasprzaka 44/52, 01-224 Warsaw, Poland

Corresponding authors: mtavakol@mit.edu (M.M.T), jingkong@mit.edu (J.K.)

Abstract

The presence of surface and grain boundary defects in organic–inorganic halide perovskite films can be detrimental to both the performance and operational stability of perovskite solar cells (PSCs). Here, we study the effect of chloride additives on the bulk and surface defects of the mixed cation and halide PSCs. We find that using an anti-solvent technique, the perovskite film is divided into two layers, i.e., a bottom layer with large grains and a thin capping layer with small grains. The addition of formamidinium chloride (FACl) into the precursor solution removes the small-grained perovskite capping layer and suppresses the

formation of bulk and surface defects, providing a perovskite film with enhanced crystallinity and large grain size of over 1 μm. Time-resolved photoluminescence measurements show longer lifetimes for perovskite films modified by FACl and subsequently passivated by 1-adamantylamine hydrochloride (ADAHCl) as compared to the reference sample. Impedance spectroscopy measurements show that these treatments reduce the charge carrier recombination in the PSCs, leading to a champion device with power conversion efficiency of 21.2% and a V_{oc} of 1152 mV under AM1.5 solar spectrum, and with negligible hysteresis during current-voltage sweeps. The Cl treated PSC also shows improved operational stability with only 12% PCE loss after 700 h under continuous illumination.

Keywords: Perovskite, Mixed cation, Solar cell, Chloride additives, Efficiency, Stability

Introduction

Inorganic-organic perovskite solar cells (PSCs) are presently studied by many research groups aiming to develop the next generation of photovoltaic devices.[1-3] Due to their low-cost and low-temperature processability, excellent light absorption, long carrier diffusion length, and high carrier mobility, perovskite materials have emerged as an exceptional candidate for optoelectronic applications.[4-8] In the last few years, much research has sought to improve the performance and operational stability of the PSCs through interface engineering, crystal engineering, compositional engineering, and passivation techniques aimed at mitigating the bulk and surface trap states of the perovskite active layer, which resulted in a record certified PCE of up to 23.7%.[9-19]

To date, many methods have been reported for fabrication of highly efficient PSC devices, including spin-coating, thermal evaporation, chemical vapor deposition (CVD), and spray coating.[20-25] Among spin-coating techniques, the anti-solvent method is one of the most

commonly used for fabrication of highly efficient mixed-cation and halide PSCs.[26-29] Perovskite films prepared using this technique possess small grains on the surface due to the fast crystallization process.[30,31] Consequently, the reduction in grain size leads to an increase in the number of grain boundaries, and in turn an increased number of potential recombination sites present at the perovskite surface.[18,32] To overcome this issue, many groups have used molecular additive engineering techniques, such as addition of modulating agents to the anti-solvent or perovskite precursor solution as well as surface passivation of the perovskite films.[33-36] A large variety of additives have been examined, e.g., polymers, organic halide salts, inorganic acids, fullerene, metal halides, co-solvents, and nanoparticles, which modify the crystallinity of the perovskite film or affect the optical and electrical properties of the perovskite absorber layer.[11] For example, Yang *et al.* modified the composition of the single A-cation perovskite bulk by adding methylammonium chloride into the perovskite solution. They improved the perovskite film crystallinity, resulting in PSCs with average PCEs of 18.55% and 17.33% for small and large-scale devices, respectively.[37,38] Zhang et al. focused on perovskite surface passivation by treating perovskite films using quaternary ammonium halides such as choline chloride, which effectively passivated the ionic defects to enable a stable PSC device with a certified PCE of 20.59%.[39]

In this work, we study the role of the anti-solvent method on perovskite crystallinity and leverage a combination of chloride additives to passivate both the perovskite bulk and surface in order to fabricate high quality mixed cation and halide perovskite solar cells. We find that a thin capping layer of perovskite with small grains is formed on top of the bulk perovskite film upon applying anti-solvent. To address this issue, some researchers previously reported addition of methylammonium chloride (MACl) or $PbCl_2$ into the perovskite composition.[37-40] Here, we select FACl as another alternative for chlorine source with better solubility than

other precursors and higher sublimation temperature than MACl helping on the higher crystallinity. Moreover, FACl helps to replace the MA cations by the FA ones and improves the crystallinity and stability of the perovskite. It can form a perovskite film with a composition close to pure $FAPbI_3$, which is an ideal case for fabrication of highly efficient PSCs.[41,42] Therefore, we add an optimum amount of FACl into the precursor solution of the perovskite and improve the perovskite crystallinity and grain size, leading to longer carrier lifetime and reduced carrier recombination in this layer. Upon annealing, Cl leaves the perovskite surface and creates surface defects. We therefore further treat the surface of the perovskite film with another Cl additive, 1-adamantylamine hydrochloride (ADAHCl). Adamantane and its derivatives are crystalline solids that have previously been used as high-density self-assembled monolayers for passivation in optoelectronic devices.[18] Because adamantane-based materials are both transparent across the solar spectrum and soluble in nonpolar organic solvents, they can be cast on top of perovskite films without dissolving the perovskite underlayer and without contributing to parasitic absorption in perovskite solar cells. We observe that subsequent passivation of the perovskite surface with 1-adamantylamine hydrochloride (ADAHCl) further improves the perovskite film quality by retarding surface recombination, as shown by PL and EIS measurements. Based on these modifications, a SnO_2-based planar PSC was achieved with a PCE of 21.2 %, low hysteresis, and high open circuit voltage of 1152 mV. The Cl treated PSC retains 88% of its initial PCE after 700 h aging under continuous illumination, which is much better than the reference device, maintaining 67% of its initial PCE value.

Results and discussion

The triple A-cation mixed-halide (ABX$_3$) perovskite composition "CsMAFA" (cesium, methylammonium, and formamidinium) is employed as a reference system and deposited using the anti-solvent technique. Here, we study the effect of chloride additives on the surface morphology and the photovoltaic performance of CsMAFA perovskite. Figure 1a and 1b illustrate schematically perovskite films deposited onto a SnO$_2$ electron transporting layer (ETL) using the antisolvent method after annealing without and with the FACl additive. The antisolvent method produces a perovskite film with small grains on the surface, as observed from the scanning electron microscopy (SEM) cross-sectional view of the reference perovskite, showing the presence of a capping layer with small grains on the top of a 300-nm-thick perovskite layer (Figure 1d). We expect this morphology to increase the charge recombination rate at the surface of the perovskite layer due to the presence of many grain boundaries and hence many grain boundary defects.

To avoid forming this capping layer, we incorporate FACl into the perovskite precursor solution which slows the perovskite crystallization process[40] and yields smooth perovskite films with large grains, as shown in Figure 1c (schematic) and Figure 1e (SEM) (for more details of the perovskite film preparation see the Experimental Section). While perovskites are typically unable to be annealed at temperatures above 100 °C without decomposing, we find that addition of FACl into the perovskite precursor solution enables us to raise the annealing temperature up to 150 °C without causing decomposition.[17,40] It was demonstrated previously that while the extra amount of FA or MA exists in the film, the high temperature annealing can enlarge the grain size and the chlorine atoms can help removing extra amount of MA or FA in the form of MACl/FACl after a period of annealing time due to their lower sublimation temperature.[21] Figure S1 shows the thermogravimetric analysis (TGA) curves of MACl, FACl and FAI powders, indicating their weight loss upon changing the temperature.

As seen, MACl sublimes and loses weight at lower temperatures than FACl or FAI, indicating that Cl atoms most likely leave the perovskite film during the annealing process in the form of MACl. Please note that the sublimation temperatures of these precursors, inside a thin film perovskite, with a high surface-to-volume ratio are lower than those temperatures shown in Figure S1. As a result, using FACl modification, we not only improve the perovskite crystallinity but also reduce the amount of MA cation in the perovskite composition, which can improve the stability of PSC devices as well.[43] To further support this claim, solution ^{1}H nuclear magnetic resonance (NMR) spectroscopy for both reference and FACl perovskite films is performed and the MA and FA peaks are studied. As shown in Figure S2, the MA (3H, NH_3) peak intensity for the FACl perovskite (located at 7.46 ppm)[44] is negligible as compared to the reference perovskite, while its FA peaks shows stronger signal as compared to those of the reference sample. These results confirm that the MA cations leave the FACl perovskite film during the annealing step at 150 °C. In addition to the NMR results, we analyze the composition of FACl perovskite film using x-ray photoelectron spectroscopy (XPS), as shown in Figure S3. We find that there is not any trace of chlorine atoms inside of the FACl perovskite film even after Ar etching of the perovskite surface for 5 times. This indicates that most of the Cl atoms leave the FACl perovskite film upon annealing at 150 °C. Based on the NMR and XPS results, we can conclude that the Cl atoms leave the perovskite film in form of MACl and consequently, addition of FACl into the perovskite composition can reduce the amount of MA cations inside a triple A-cation perovskite and improve the quality and the stability of the perovskite film.

Top-view SEM images of perovskite films fabricated without and with the FACl additive are shown in Figure 2a and 2b, respectively. These results confirm that upon addition of FACl, the average perovskite grain size is increased from 180 nm to 720 nm. We further employ

2

atomic force microscopy (AFM) to study the surface roughness and morphology of the resulting perovskite films (Figure 2c-d). AFM results also show that the grain size of perovskite film is increased by addition of FACl, which is in good agreement with SEM results. Moreover, we found that the surface roughness in the perovskite films is reduced from 40±4 nm to 31±5 nm by including the FACl additive (Figure S4), providing a smoother interface in contact with the HTL.

Figure 3a and 3b show the two-dimensional X-ray diffraction (2D-XRD) patterns of the perovskite films without and with the FACl additive, both with similar thickness of 400 nm. The diffraction patterns of the corresponding films after integration are shown in Figure 3c. The significant peaks located at $2\theta = 14.24°$, 28.65°, 31.92°, 43.85° correspond to the (110), (220), (310), and (330) planes, respectively, confirming the formation of a perovskite film with tetragonal structure[21] in the case of both perovskite films. We find that the intensity of the diffraction peaks for the perovskite film with FACl is significantly increased, consistent with the better crystallinity.

We also observe that the (110)-to-(310) peak intensity ratio in the FACl perovskite is 1.82 compared to 0.95 for the reference sample, indicating that the FACl treated-perovskite is mostly oriented along the out-of-plane (110) direction and more oriented than the film fabricated without Cl additives. We note that the FACl sample contains a trace of PbI_2 peak at 13.8°, which is due to the higher temperature annealing process. As reported in the literature, an extra amount of PbI_2 is beneficial to obtaining high performance devices.[3]

From the results discussed above, the FACl additive can improve the crystallinity and quality of bulk perovskite. However, PSCs mostly suffer from carrier recombination at the interfacial regions, as reported by many groups.[11,17,18] Consequently, surface treatment of the perovskite

2

film is another effective strategy to further boost device performance and stability. Here, we employ Cl-based adamantane, *i.e.*, ADAHCl, for surface passivation of the perovskite. Figure 4 shows the optical properties of the resulting perovskite films without and with Cl additives. All samples exhibit almost similar absorption onsets and photoluminescence peak positions (band gap is around 1.61 eV) indicating that the chlorine atoms are removed from the film during the annealing process at 150°C due to the volatile nature of MACl.[17] However, the PL intensity of the perovskite film with Cl additive is stronger than the reference sample, which can be attributed to higher quality of the film and larger grains. It is also consistent with the time-resolved PL (TRPL) results shown in Figure 4b. We extract a 17.5 ns carrier lifetime for the reference sample, which is shorter than that of the FACl-based perovskite film with 22.3 ns lifetime. Moreover, we observe that the lifetime for FACl-based perovskite is further enhanced to 28.6 ns after passivation of the surface defects by ADAHCl. To further study the role of Cl additives, PL intensity maps of perovskite films are measured, as shown in Figures 4c-4e. The resulting maps indicate that while FACl incorporation improves PL intensity and uniformity compared to the reference sample, the perovskite film with both FACl and ADAHCl passivation shows the strongest and most uniformly-distributed PL intensity. These results show that the perovskite films with both bulk and surface modification have higher quality and the recombination sites in these perovskites caused by the anti-solvent technique have been effectively passivated.

In order to study the effect of Cl additives on photovoltaic properties, we fabricate solar cell devices with a planar configuration of FTO/compact SnO_2/perovskite/spiro-OMeTAD/Au, as shown in Figure 5a. The current-voltage (*J-V*) characteristics of champion PSCs without and with FACl additive, before and after passivation by ADAHCl were measured under AM 1.5G irradiation and reverse scan directions (Figure 5b). The figures of merit for the corresponding

devices are listed in Table 1. The reference device demonstrates a typical PCE of 19.43% with J_{sc} of 22.48 mA/cm^2, V_{oc} of 1110 mV, and FF of 77.8%, while the FACl-based device yields an enhanced PCE of 20.52% with a higher V_{oc} of 1134 mV and J_{sc} of 23.01 mA/cm^2. These enhancements could be originated from lower bulk recombination sites (due to larger grain size), excess amount of PbI_2, and orientational growth of perovskite crystals in the FACl device. The statistics of photovoltaic parameters for the PSCs with different concentrations of FACl are shown in Figure S5 and indicate that there is an optimum amount of FACl, *i.e.*, 10 mg in 1 mL of the reference perovskite solution.

Using ADAHCl to passivate the surface of FACl-modified perovskite further improves photovoltaic performance, leading to a champion device with PCE of 21.2%, J_{sc} of 23.4 mA/cm^2, and V_{oc} of 1152 mV. We similarly performed an optimization study on the concentration of ADAHCl for perovskite surface passivation. Figure S6 shows the statistics of photovoltaic parameters for PSCs passivated with different concentrations of ADAHCl, and we found that 3 mg/1mL (chlorobenzene) is the best concentration for this purpose. The statistical *J-V* data for PSCs without and with Cl additives are shown in Figure S7. These results show that after doing only passivation with ADAHCl, the average values of all the photovoltaic parameters are increased as compared to those of the reference devices. However, these enhancements are not as high as those of the devices with FACl additive. In the FACl devices, the average values of the J_{sc}, FF, and PCE are higher than those of devices with passivation. Only the average value of V_{oc} for the passivated devices with ADAHCl is slightly better than devices with FACl. It is worth pointing out that by applying both modifications at the same time, all the photovoltaic parameters are increased even more than those of either FACl devices or the passivated devices, indicating the importance of those modification for the PSC devices. We find that addition of both FACl and ADAHCl additives

into the perovskite film at the same time improves the average values of J_{sc} and especially the V_{oc} (up to 1142 mV).

Table 1. Figures of merit for the champion PSC devices under reverse scan direction

Sample	V_{oc} (mV)	J_{sc} (mA/cm^2)	FF (%)	PCE (%)	J_{sc} from EQE (mA/cm^2)
Reference	1110 (1107)	22.48 (22.4)	77.8 (75.3)	19.43 (18.65)	21.2
With FACl	1134 (1125)	23.01 (22.82)	78.5 (76.8)	20.52 (19.7)	22.12
With FACl and ADAHCl passivation	1152 (1142)	23.4 (22.9)	78.3 (77.3)	21.2 (20.15)	22.65

*Note that the average values of PSC parameters are presented in the bracket.

In addition to *J-V* curves, we measured the maximum power point tracking (MPPT) and the external quantum efficiency (EQE) of the corresponding devices to confirm the PCE stability of the devices over time and J_{sc} improvement achieved by applying Cl additives, respectively. Figure S8 shows the stabilized maximum power point of the reference cell, FACl device without and with passivation after one minute are 19.22%, 20.32%, and 21.01%, respectively.

As shown in Figure 5c, it is clear that the EQE response of the reference cell is indeed increased by incorporation of the FACl additive into the perovskite precursor solution and by subsequent surface passivation of the perovskite film with ADAHCl. The calculated J_{sc} from EQE results were 21.2, 22.12, and 22.65 mA/cm^2, respectively, which are in good agreement with the values measured in the *J-V* curves (Figure 5b). In order to study the role of Cl additives on hysteresis, we measured 10 devices from each condition under forward and backward scan directions. The statistics of hysteresis index (Hysteresis index = ((PCE$_{backward}$-

2

$PCE_{forward})/PCE_{backward}) \times 100)$ for the corresponding PSCs are shown in Figure S9. As seen, the FACl-containing device and ADAHCl passivated device have lower average hysteresis indices as compared to the reference PSCs, which has previously been correlated with the higher perovskite quality and lower defect density.[45]

Recent works demonstrated that due to the organic nature of perovskites and unbonded surface atoms, the surface of the perovskite film – even with large grains – is vulnerable to moisture and sunlight.[4] One of the main current challenges in the field of PSCs is thus achieving long-term stability under light and humidity, which is crucial for commercialization. We therefore examined the effect of FACl and ADAHCl additives on devices stability by keeping the PSCs in a dry air box (relative humidity (RH) of 40%) and periodically recording *J-V* scans over 90 days. Our results show an improved stability for FACl- and ADAHCl-treated devices (95% of initial PCE retained after 90 days) as compared to FACl-treated PSCs (91%) and reference untreated samples (86.5%) (Figure 5d).

To get a better insight into the device stability after Cl treatment, we analyzed the surface of perovskite films using contact angle measurements. Interestingly, the contact angle of water droplet is increased from 48° to 67° after Cl treatment, suggesting less wetting by water for the Cl treated perovskite film. Herein, adamantane part plays a significant role and changes the surface properties of the perovskite film. In fact, a thin layer of ADAHCl on top of the perovskite film works as a protection layer with water-repellent properties, resulting in a better stability in our devices.

Additionally, we measured the operational stability of reference and Cl-treated PSCs under continuous illumination at maximum power point tracking. This measurement was performed at room temperature under nitrogen flow, as shown in Figure 6c. The Cl-treated device

retains 88% of its initial PCE value after 700 h under continuous illumination, while the reference device maintains only 67% of its PCE under the same condition. This highlights the impact of the Cl treatment on not only shelflife stability but also the operational stability of the PSC devices.

To further understand the role of the Cl additives, electrochemical impedance spectroscopy (EIS) measurements were carried out for PSCs without and with Cl additives (both FACl and ADAHCl) under illumination as a function of applied bias (0 to V_{oc} of devices) and frequency (200 mHz to 2MHz). Figures 7a and S11 show the EIS spectra of devices measured under zero applied bias and the corresponding electrical equivalent circuit, respectively. The detailed description of the electrical equivalent circuit has been discussed in our previous work, which is the most commonly employed circuit for describing the working mechanism of PSCs.[32] Briefly, the resistive and capacitive components of the electrical equivalent circuit can be described as follows:

- Rs represents the series resistance due to the DC resistance of PSCs and connecting wires.

- R_1, C_1 are the high frequency resistance and capacitance, respectively. R_1 is identified as leakage resistance under low forward bias or recombination resistance at high forward bias, whereas capacitance (C_1) is due to the dielectric properties of the absorber layer.

- R_{rec} and C are the low frequency resistance and capacitance, respectively. The exact origin of the low frequency resistance is still unknown but mostly it is correlated with the recombination. The capacitance C results from the accumulation of charge and ions at either the ETL/perovskite or the perovskite/HTL interface.

The Nyquist spectrum shown in Figure 7a depicts the contribution from two different mechanisms. From the intersection of high frequency imaginary impedance on the X-axis, the

2

values of R_s have been calculated and found to be 12.4 Ω and 10.2 Ω for PSCs without and with Cl additives, respectively. A lower value of R_s is expected for Cl-based PSCs as they exhibit larger grain sizes that could reduce the resistance offered by grain boundaries. The extracted values of high frequency resistance for both devices are shown in Figure 7b. A higher value of R_1 for Cl-based device indicates lower recombination in this device. Figure 7c shows the variation of R_{rec} with respect to applied bias extracted from Nyquist spectra for both samples. A higher value of recombination resistance R_{rec} for Cl-based PSCs compared to the reference PSC signifies the lower recombination in the Cl-treated devices. The R_{rec} of both devices can also be understood from the expression of $R_{rec} = \frac{nK_BT}{qj_s}\exp(-\frac{qV}{nK_BT})$, where n, K_B, T, q, J_s, and V are ideality factor, Boltzmann constant, temperature, charge, reverse saturation current, and applied bias, respectively.[36] By using the above expression and the data from Figure 7c, we extract ideality factors of 2.1 and 1.8 for PSCs without and with Cl additives, respectively. These results are consistent with our PL results and suggest reduced recombination is the predominant reason for enhanced *J-V* performance in the PSCs with Cl additives. The ideality factors of both PSCs without and with Cl additives were also calculated from the dark *J-V* characteristics (Figure 7d). The details and procedures for the calculation of the ideality factor from dark *J-V* curves have been discussed in detail in our previous work.[32,36] Figure 7d shows the calculated values of ideality factors for both devices. From dark current curves, values of 2 and 1.6 have been extracted for PSCs without and with Cl additives, respectively.

Conclusions

In summary, we studied the role of Cl additives on the morphology and film quality of mixed cation and halide PSCs fabricated using the anti-solvent method. We find that the anti-solvent

technique induces the formation of small grains on the surface of the perovskite layer due to the fast nucleation and consequently may increase the charge recombination rate at the interfacial regions. Molecular additive engineering using FACl leads to the formation of perovskite films with smoother surfaces and larger grains, which can reduce the charge recombination at the interfaces and improve the performance of PSCs. Moreover, we demonstrate that surface modification of perovskite films using ADAHCl further improves the film quality and retards the surface recombination rates. Modification of the perovskite film with the combination of these chloride additives results in efficient planar PSCs with high PCE of 21.2%, V_{oc} of 1152 mV, and lower hysteresis than untreated control samples. In addition, Cl-treated devices demonstrate improved operational stability with only 12% PCE loss under continuous illumination after 700 h aging. Our work develops an efficient combined bulk and surface modification approach using molecular Cl additives in contrast to the anti-solvent technique and suggests further enhancements both in the efficiency and stability of PSCs.

Experimental Section

Device fabrication

Fluorinated-tin-oxide (FTO) coated glass substrates (Nippon Sheet Glass 10 Ω/sq (NSG-10)) are etched by zinc powder and diluted HCl to define the electrode patterns and then cleaned in triton X100 (1 vol% in deionized water) using the ultrasonic bath for 20 min, and rinsed in DI water, acetone, and ethanol, in sequence. This is followed by the UV ozone cleaning, after which the substrates are coated with an SnO_2 solution ($SnCl_4.5H_2O$ diluted in ethanol (0.03 M)) that is spin-coated twice at 4000 rpm for 20 s and followed by annealing at 180°C for 60 min. Next, the SnO_2 film is treated by using a chemical bath deposition technique. First, 0.5 g

urea, 10 mL mercaptoacetic acid and 0.5 mL HCl (37%) are mixed in 40 mL DI water. Then, $SnO_2 \cdot 2H_2O$ is dissolved in the solution at 0.005 M concentration. The SnO_2 films are placed into the bath solution and kept in an oven at 70 °C for 1 h. These substrates are then cleaned again and then annealed at 180 °C for 1 h.

Perovskite film is deposited by using a precursor solution of $(FAPbI_3)_{0.87}(MAPbBr_3)_{0.13}$ perovskite prepared by dissolving FAI (1.05 M, Dyesol), PbI_2 (1.10 M, TCI), MABr (0.185 M, Dyesol) and $PbBr_2$ (0.185 M, TCI) in mixed solvents of DMF:DMSO = 4:1 (volume ratio). Afterward, a solution of CsI (1.5 M in DMSO) is prepared and 5 vol% of CsI solution was added to the solution to have a triple A-cation perovskite. To prepare FACl-based perovskite, 0-25 mg of FACl was added into 1 mL of reference perovskite. For deposition, the solution was spin-coated in two steps: 1000 rpm for 10 s and 6000 rpm for 30 s (ramp rate: 2000 rpm/s). In order to apply chlorobenzene (CB) as an anti-solvent, 200 µL of CB is dropped on the surface of the film for 10 seconds before the end of spinning. After deposition, the reference perovskite is annealed at 120 °C and 100 °C for 10 min and 40 min, respectively. For perovskite films with the FACl additive, the annealing process is performed at 150 °C for 20 min and at 100 °C for another 30 min. After the annealing process of the perovskite film, a solution of ADAHCl in CB (3 mg/1 mL) is spin-coated on the film at 4000 rpm for 20 s, followed by annealing at 100 °C for 10 min. Afterward, a solution of spiro-OMeTAD (70 mM) in 1 mL CB is prepared by adding 18 µL of 4-tert-butylpyridine (4tBP-Sigma-Aldrich) and 32 µL from the solution of bis(trifluoromethylsulfonyl)imide lithium salt (Li-TFSI, Sigma-Aldrich) in acetonitrile (1.8 mM). The HTL solution is spin-coated on top of perovskite at 4000 rpm for 20 s (with ramp rate of 2000 rpm/s). Finally, the device is completed by thermal evaporation of 100 nm-thick gold layer as a back-contacted electrode.

Film characterization

Scanning electron microscopy (HRSEM) and x-ray diffraction (XRD) patterns are recorded by a ZEISS Merlin high resolution SEM/ a focused ion beam (FIB, Helios) and a Bruker D8 X-ray Diffractometer (USA) with GADDS utilizing a Co radiation, respectively. To measure the average grain size, 6 SEM images from each perovskite were considered and the average grain size was estimated using Clemex. UV–visible and photoluminescence (PL) spectra are measured by a Varian Cary 5 and a Fluorolog 322 (Horiba Jobin Ybon Ltd), respectively. The collected PL is in the wavelength range of λ=620 nm to λ=850 nm with excitation at λ=460 nm. A picosecond pulsed diode laser (EPL-405, with excitation wavelength of λ=405 nm and pulse width of 49 ps) is used to record time-resolved PL (TRPL). The obtained data is fitted by using a biexponential equation ($I(t) = a_i \exp(-t/\tau_i)$), where a_i and τ_i are the amplitude and the lifetime of each exponential component, respectively. The average lifetime (τ_{avr}) is estimated from $\tau_{avr} = a_1\tau_{1*}a_2\tau_2/(a_1\tau_1+a_2\tau_2)$. Atomic force microscopy (AFM) is measured by NanoScope IIIa/Dimension 3100. Ultraviolet photoelectron spectroscopy (UPS) is performed in an Omicron ultrahigh vacuum system using the He I line (21.2 eV) of a helium discharge lamp to study the Fermi level and valence bands of different layers. Thermogravimetric analysis is measured using (TGA, UNIX/TGA7 (PerkinElmer)) and the heating and cooling rates were 10 °C/min. Contact angle of water droplet was measured using Dataphysics OCA 20. An x-ray photoelectron spectrometer (ESCALAB 250Xi, Thermo Fisher Scientific Inc., USA) with Al Kα radiation (hν = 1486.6 eV) was employed to measure x-ray photoelectron spectroscopy (XPS) spectra. A Bruker 600 AVANAC III spectrometer equipped with Bruker BBO multinuclear probe (BrukerBioSpin, Rheinstetten, Germany) was employed to measure ^{1}H NMR at 298 K. For this measurement, the perovskite films were dissolved in DMSO-d6 and the MA and FA peaks were analyzed.

Device measurement

For device measurement, a digital source meter (Keithley model 2400, USA) and a 450 W xenon lamp (Oriel, USA) are used. The spectral output of the lamp is filtered using a Schott K113 Tempax sunlight filter (Präzisions Glas & Optik GmbH, Germany) to match the emission spectra of the lamp to the AM1.5G standard. For measurements a black mask with 0.16 cm^2 opening, corresponding to the active area of each device, is placed over the device. During the measurement, the voltage scan rate and the dwell time are 10 mV/s and 15 s, respectively. The light intensity is adjusted to 1000 W/m^2 in accordance with standard AM 1.5 reporting conditions. For calculation of the hysteresis index the following formula is used: Hysteresis index = (($PCE_{backward}$-$PCE_{forward}$)/$PCE_{backward}$)*100. A commercial apparatus (Arkeo-Ariadne, Cicci Research s.r.l.) with a 300 Watts Xenon lamp are employed to measure External quantum efficiency (EQE) spectra. For impedance spectroscopy (IS), DC bias range is adjusted from 0 to open circuit voltage of the devices, with an AC perturbation signal of 20 mV. The frequency is changed from 200 mHz to100 kHz.

A Biologic MPG2 potentiostat together with white LED lamp were employed to simulate standard AM 1.5G condition. The stability test was measured at the maximum power point (MPP) under continuous illumination and nitrogen flow. Before starting the experiment, we purged nitrogen gas for an hour to remove the residual oxygen and water from the holder. The MPP was measured and updated every 60 s. A Peltier element was used to control the substrate temperature during the test. The temperature was fixed to 25 °C during the test.

Acknowledgment

References

1. M. Grätzel, *Nat. Mater.* **2014,** *13*, 838-842.

2. N. J. Jeon, H. Na, E. H. Jung, T. Y. Yang, Y. G. Lee, G. Kim, H. W. Shin, S. I. Seok, J. Lee, J. Seo, *Nat. Energy* **2018,** *3*, 682.

3. W. S. Yang, B. W. Park, E. H. Jung, N. J. Jeon, Y. C. Kim, D. U. Lee, S. S. Shin, J. Seo, E. K. Kim, J. H. Noh, S. I. Seok, *Science* **2017,** *356*, 1376-1379.

4. M. M. Tavakoli, W. Tress, J. V. Milić, D. Kubicki, L. Emsley, M. Grätzel, *Energy Environ. Sci.* **2018,** *11* 3310.

5. D. Y. Son, J. W. Lee, Y. J. Choi, I. H. Jang, S. Lee, P. J. Yoo, H. Shin, N. Ahn, M. Choi, D. Kim, N. G. Park, *Nat. Energy* **2016,** *1***,** 16081.

6. Q. Lin, L. Lu, M. M. Tavakoli, C. Zhang, G. C. Lui, Z. Chen, X. Chen, L. Tang, D. Zhang, Y. Lin, P. Chang, *Nano Energy* **2016,** *22*, 539-547.

7. S. F. Leung, Q. Zhang, M. M. Tavakoli, J. He, X. Mo, Z. Fan, *Small* **2016,** *12,* 2536-2548.

8. M. M. Tavakoli, K. H. Tsui, Q. Zhang, J. He, Y. Yao, D. Li, Z. Fan, *ACS Nano* **2015,** *9*, 10287-10295.

9. J. Burschka, N. Pellet, S. J. Moon, R. Humphry-Baker, P. Gao, M. K. Nazeeruddin, M. Grätzel, *Nature,* **2013,** *499*, 316.

10. A. Ng, Z. Ren, Q. Shen, S. H. Cheung, H. C. Gokkaya, S. K. So, A. B. Djurišić, Y. Wan, X. Wu, C. Surya, *ACS Appl. Mater. Interfaces* **2016,** *8*, 32805.

11. T. Li, Y. Pan, Z. Wang, Y. Xia, Y. Chen, W. Huang, *J. Mater. Chem. A* **2017,** 5, 12602-12652.

12. J. Shi, H. Zhang, X. Xu, D. Li, Y. Luo, Q. Meng, *Small* **2016,** *12*, 5288.

13. M. M. Tavakoli, F. Giordano, S. M. Zakeeruddin, M. Grätzel, *Nano Lett.* **2018,** *18*, 2428-2434.

14. M. M. Tavakoli, R. Tavakoli, Z. Nourbakhsh, A. Waleed, U. S. Virk, Z. Fan, *Adv. Mater. Interfaces* **2016**, 3 1500790.

15. H. Chen, F. Ye, W. Tang, J. He, M. Yin, Y. Wang, F. Xie, E. Bi, X. Yang, M. Grätzel, L. Han, *Nature* **2017,** *550*, 92-95.

16. M. M. Tavakoli, L. Gu, Y. Gao, C. Reckmeier, J. He, A. L. Rogach, Y. Yao, Z. Fan, *Sci. Rep.* **2015,** *5*, 14083.

17. C.Zuo, L. Ding, *Nanoscale* **2014,** *6,* 9935-9938.

18. M. M. Tavakoli, D. Bi, L. Pan, A. Hagfeldt, S.M. Zakeeruddin, M. Grätzel, *Adv. Energy Mater.* **2018,** *8*, 1800275.

19. J. E. Bishop, D. K. Mohamad, M. Wong-Stringer, A. Smith, D. G. Lidzey, *Sci. Rep.* **2017,** *7*, 7962.

20. M. M. Tavakoli, S.M. Zakeeruddin, M. Grätzel, Z. Fan, *Adv. Mater.* **2018,** *30*, 1705998.

21. Y. Xie, F. Shao, Y. Wang, T. Xu, D. Wang, F. Huang, *ACS Appl. Mater. Interfaces* **2015,** *7*, 12937-12942.

22. M. M. Tavakoli, A. Simchi, X. Mo, Z. Fan, *Mater. Chem. Front.* **2017,** *1*, 1520-1525.

23. M. M. Tavakoli, R. Tavakoli, P. Yadav, J. Kong, *J. Mater. Chem. A* 2019, *7,* 679-686.

24. J. E. Bishop, D. K. Mohamad, M. Wong-Stringer, A. Smith, D. G. Lidzey, *Sci. Rep.* **2017,** *7*, 7962.

25. M. M. Tavakoli, A. Waleed, L. Gu, D. Zhang, R. Tavakoli, B. Lei, W. Su, F. Fang, Z. Fan, *Nanoscale* **2017,** *9*, 5828-5834.

26. M. Konstantakou, D. Perganti, P. Falaras T. Stergiopoulos, *Crystals*, **2017**, *7*, 291.

27. M. Saliba, T. Matsui, K. Domanski, J.-Y. Seo, A. Ummadisingu, S. M. Zakeeruddin, J.-P. Correa-Baena, W. R. Tress, A. Abate, A. Hagfeldt, M. Gratzel, *Science*, **2016**, *354*, 206–209.

28. M. Yavari, M. Mazloum-Ardakani, S. Gholipour, M. M. Tavakoli, S. H. Turren-Cruz, N. Taghavinia, M. Grätzel, A. Hagfeldt, M. Saliba, *Adv. Energy Mater.* **2018**, *8*, 1800177.

29. N. Ahn, D.-Y. Son, I.-H. Jang, S. M. Kang, M. Choi, N.-G. Park, *J. Am. Chem. Soc.*, **2015**, *137*, 8696–8699.

30. D. Prochowicz, M. M. Tavakoli, A. Solanki, T. W. Goh, K. Pandey, T. C. Sum, M. Saliba, P. Yadav, *J. Mater. Chem. A* **2018,** 6, 14307-14314.

31. N. J. Jeon, J. H. Noh, Y. C. Kim, W. S. Yang, S. Ryu, S. I. Seok, *Nat. Mater.* **2014**, *13*, 897–903.

32. P. Yadav, S. H. Turren Cruz, D. Prochowicz, M. M. Tavakoli, K. Pandey, S. M. Zakeeruddin, M. Grätzel, A. Hagfeldt, M. Saliba, *J. Phys. Chem. C* **2018,** *122*, 15149.

33. J. Xu, A. Buin, A. H. Ip, W. Li, O. Voznyy, R. Comin, M. Yuan, S. Jeon, Z. Ning, J. J. McDowell, P. Kanjanaboos, *Nat. Commun.* **2015,** *6*, 7081.

34. M. M. Tavakoli, R. Tavakoli, P. Davami, H. Aashuri, *J. Comput. Electron.* **2014**, *13,* 425-431.

35. M. M. Tavakoli, A. Simchi, H. Aashuri, *Mater. Chem. Phys.* **2015,** *156*, 163-169.

36. M. M. Tavakoli, P. Yadav, R. Tavakoli, J. Kong, *Adv. Energy Mater.* **2018,** *8*, 1800794.

2

37. M. Yang, Z. Li, M. O. Reese, O. G. Reid, D. H. Kim, S. Siol, T. R. Klein, Y. Yan, J. J. Berry, M. F. van Hest, K. Zhu, *Nat. Energy* **2017,** *2*, 17038.

38. Y. Deng, X. Zheng, Y. Bai, Q. Wang, J. Zhao, J. Huang, *Nat. Energy* **2018,** *3*, 560-566.

39. X. Zheng, B. Chen, J. Dai, Y. Fang, Y. Bai, Y. Lin, H. Wei, X. C. Zeng, J. Huang, *Nat. Energy* **2017,** *2*, 102.

40. H. Yu, F. Wang, F. Xie, W. Li, J. Chen, N. Zhao, *Adv. Funct. Mater.* **2014,** *24,* 7102-7108.

41. M. M. Tavakoli, M. Saliba, P. Yadav, P. Holzhey, A. Hagfeldt, S. M. Zakeeruddin and M. Grätzel, *Adv. Energy Mater.* **2019***, 9*, 1802646.

42. S. H. Turren-Cruz, A. Hagfeldt, M. Saliba, *Science* **2018**, *362,* 449-453.

43. Q. Li, Y. Zhao, R. Fu, W. Zhou, Y. Zhao, X. Liu, D. Yu, Q. Zhao, *Adv. Mater.* **2018,** *30*, 1803095.

44. O. J. Weber, B. Charles, M. T. Weller, *J. Mater. Chem. A* **2016**, *4,* 15375-15382.

45. Y. Lee, S. Paek, K. T. Cho, E. Oveisi, P. Gao, S. Lee, J. S. Park, Y. Zhang, R. Humphry-Baker, A. M. Asiri, M. K. Nazeeruddin*, J. Mater. Chem. A* **2017,** *5*, 12729-12734.
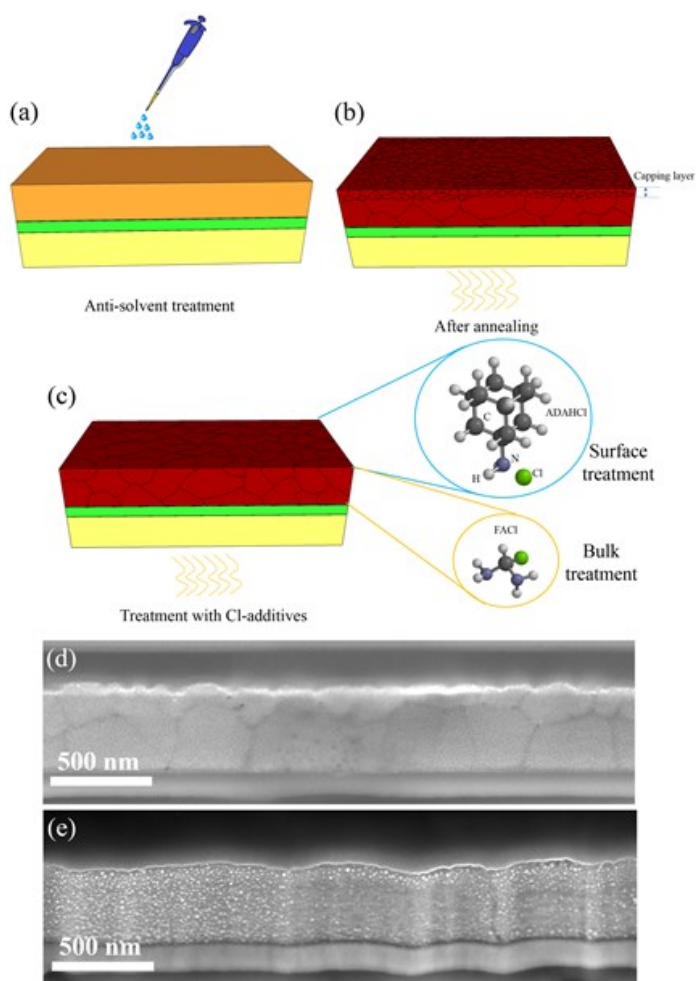
Figure 1. Schematic depiction of perovskite films fabricated by the anti-solvent method on SnO$_2$-coated FTO glass before (a) and after (b) annealing, and after treatment with Cl additives (c). Cross-sectional view SEM images of devices without (d) and with Cl additives (e), showing that Cl additives remove the capping layer of perovskite with small grains. Please note that the SEM images taken by a focused ion beam (FIB) instrument and due to applying a high energy ion beam, the perovskite layer is decomposed partially, and the white dots are PbI$_2$.
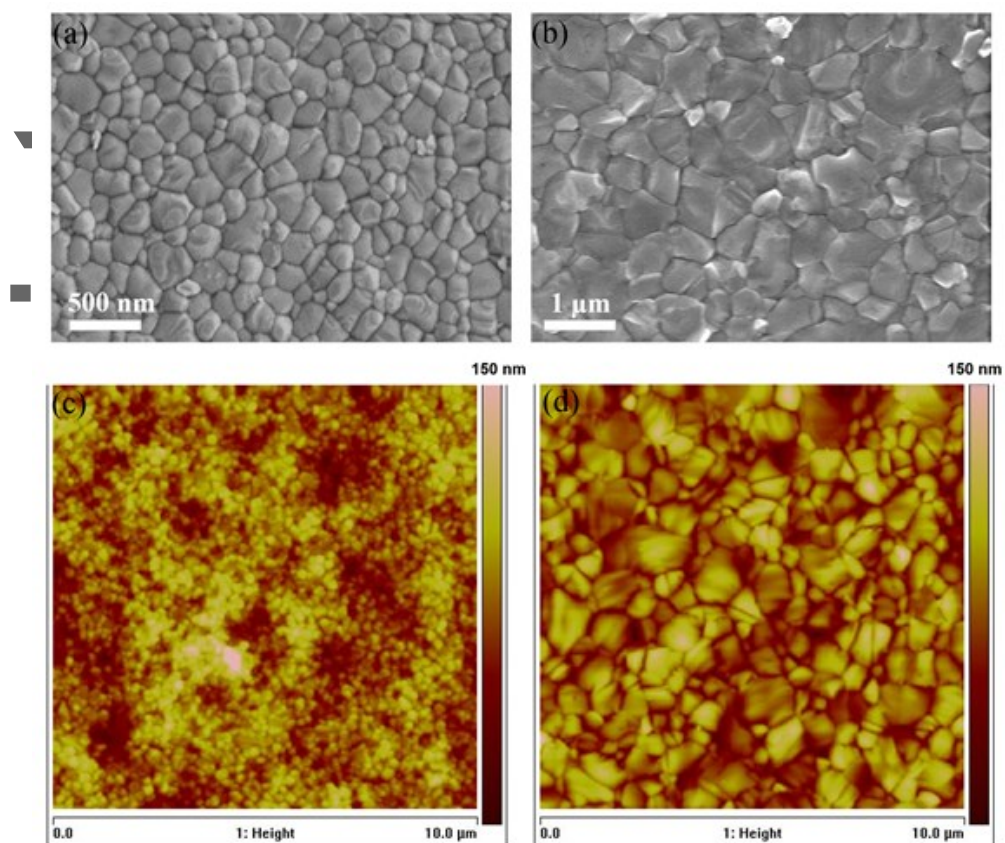
Figure 2. Top-view SEM image of perovskite films (a) reference and (b) with the FACl additive. AFM images of perovskite films (c) reference and (d) with the FACl additive.
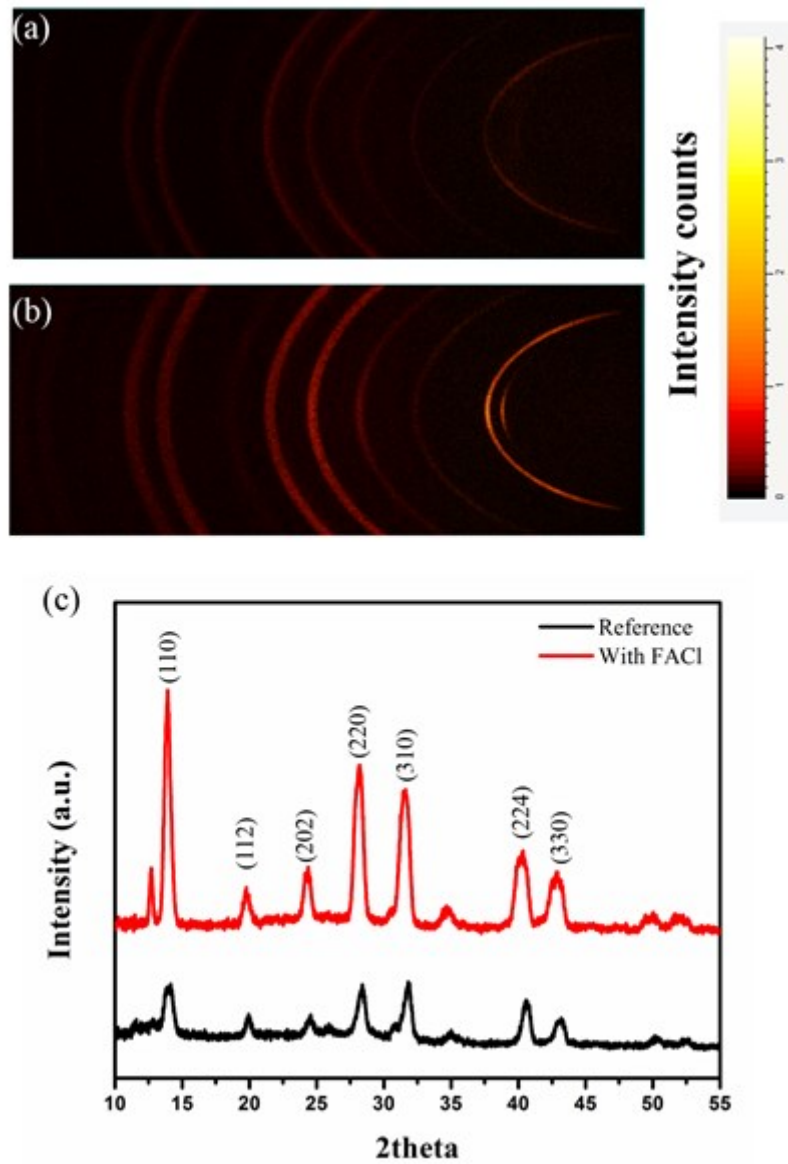
Figure 3. Two-dimensional X-ray diffraction (2D-XRD) patterns of perovskite films (a) reference and (b) with the FACl additive. (c) Peak intensity versus 2Ө by integration of the data.
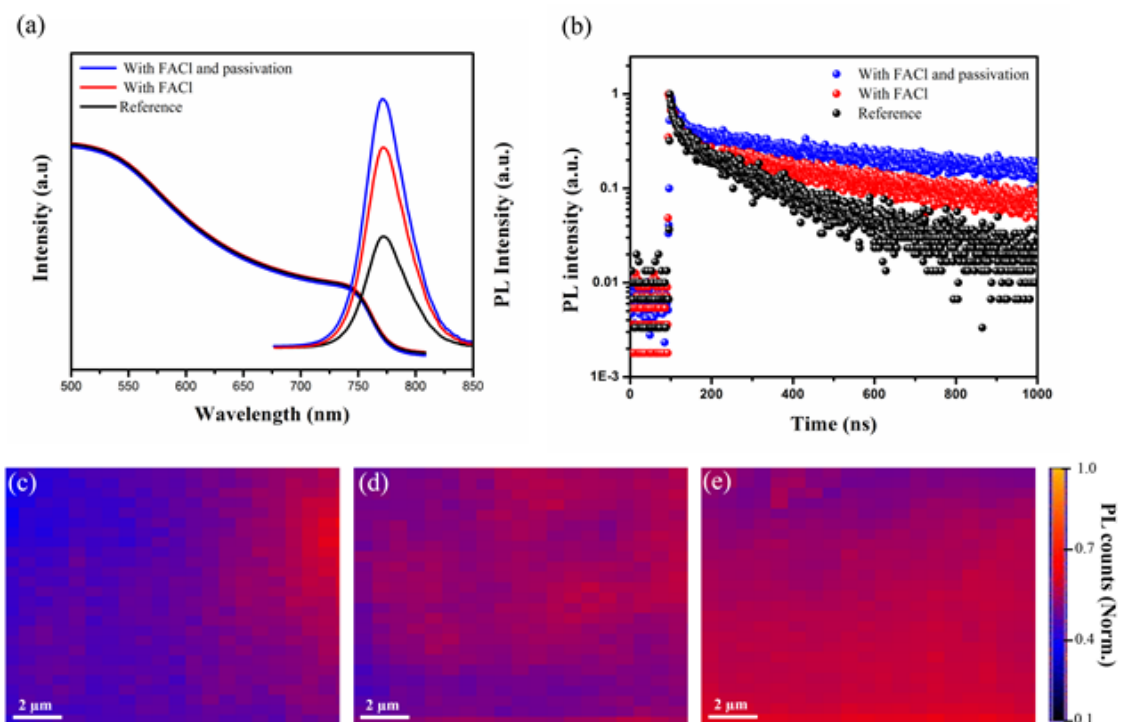
Figure 4. (a) Optical properties (UV-vis and PL spectra), and (b) time-resolved PL (TRPL) curves of perovskite films without and with Cl additive. (c), (d), and (e) PL intensity mapping of the perovskite films, corresponding to "Reference", "With FACl", and "With FACl and Passivation", respectively.
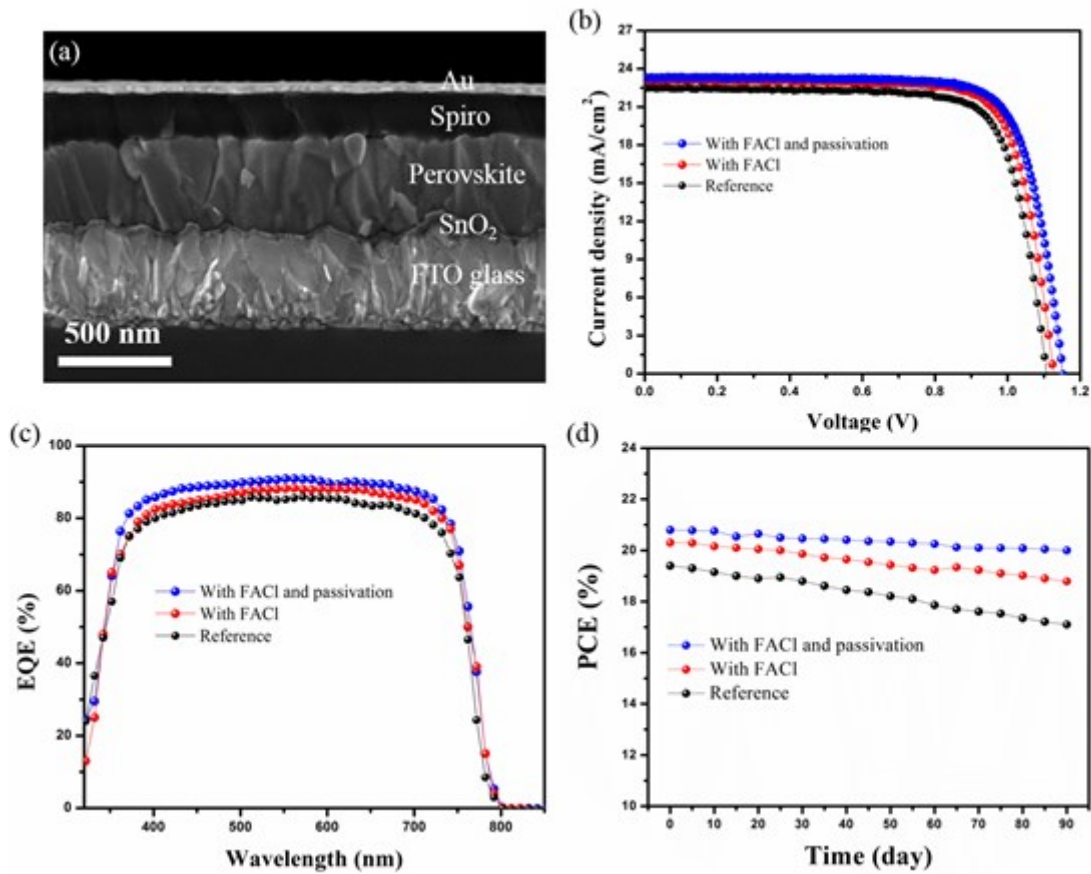
Figure 5. (a) SEM cross-section image of a PSC device with the FACl additive and after passivation with ADAHCl. (b) *J-V* curves and (c) EQE spectra of champion PSC devices (reference, with FACl additive, with FACl and after passivation). (d) Shelf life test of PSC devices kept in dry air box (RH=40%) at room temperature.

2
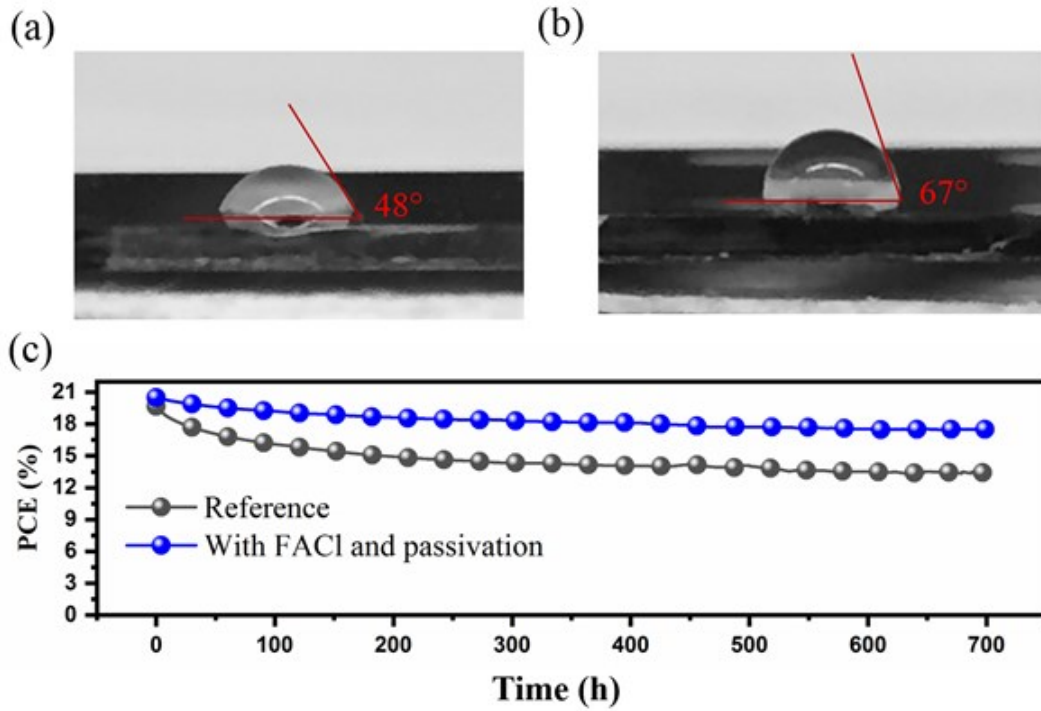
Figure 6. Contact angle measurements of a water droplet on top of the (a) reference and (b) Cl-treated perovskite films. (c) Stability test of the corresponding PSCs at room temperature for 700 h under continuous full sun illumination and at maximum power-point tracking.
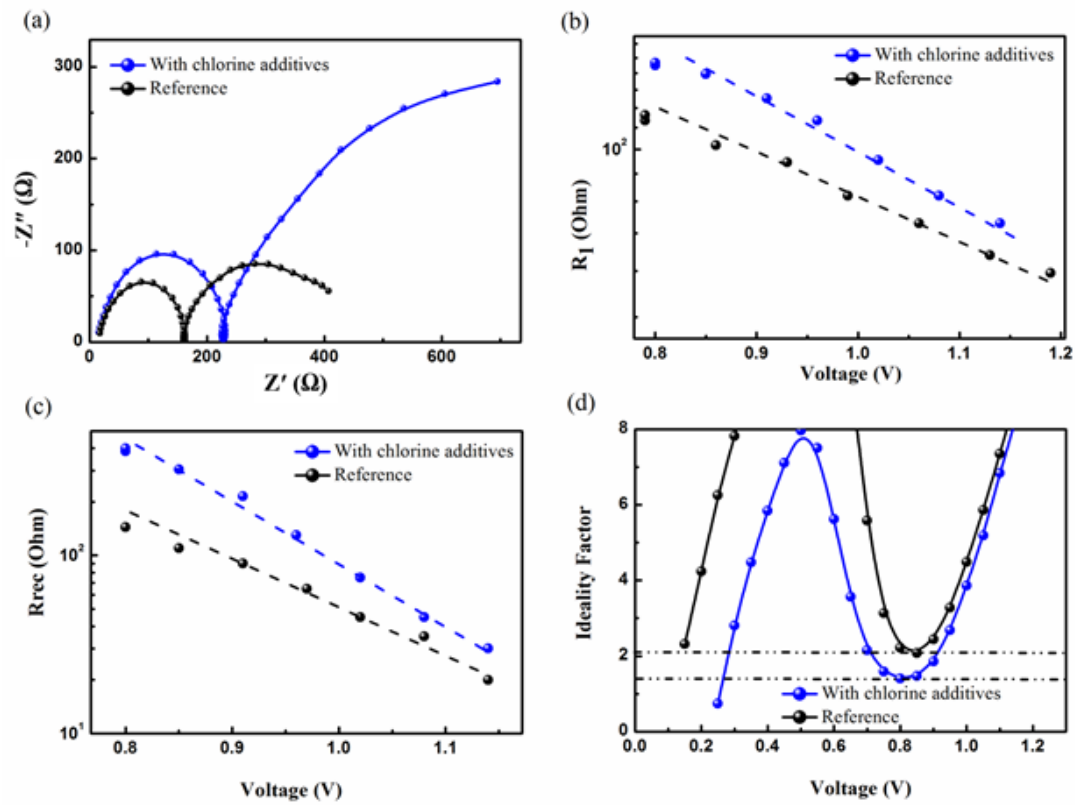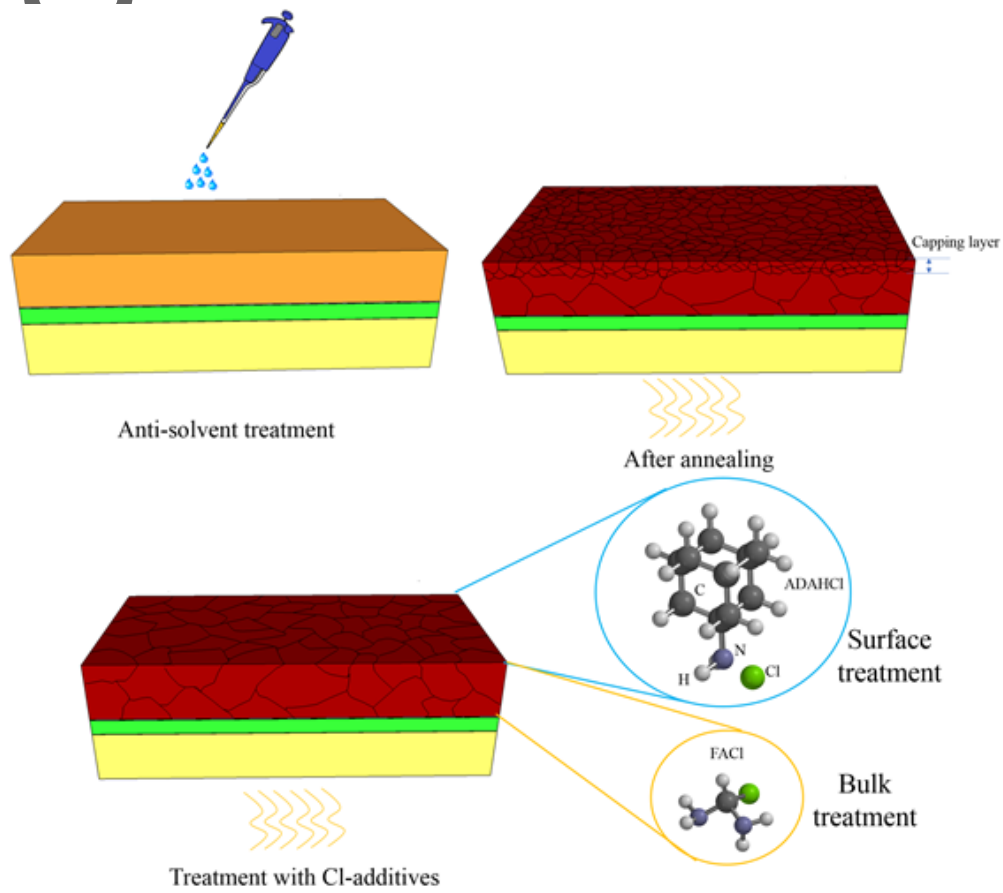
Figure 7. (a) EIS spectra of PSCs without and with Cl additives (FACl and ADAHCl) measured under 1 Sun illumination, AM1.5 spectrum. (b) High frequency resistance and (c) Low frequency resistance extracted from Nyquist spectra by using electrical equivalent circuit for reference PSC and device with Cl additives. (d) Ideality factor versus voltage for the corresponding devices.

TOC

Molecular additive engineering using chlorine-based compounds such as FACl reduces the bulk and surface carrier recombination and improves the crystallinity of the perovskite film, resulting in solar cell devices with high efficiency exeeding 21% and great stability.

2